An Analysis of Insar Displacement Vector Decomposition Fallacies and the Strap-Down Solution

Brouwer, Wietske S.; Hanssen, Ramon F.

DOI
10.1109/IGARSS47720.2021.9554216

Publication date
2021

Document Version
Final published version

Published in
2021 IEEE International Geoscience and Remote Sensing Symposium IGARSS

AN ANALYSIS OF INSAR DISPLACEMENT VECTOR DECOMPOSITION FALLACIES AND THE STRAP-DOWN SOLUTION

Wietske S. Brouwer and Ramon F. Hanssen

Department of Geoscience and Remote Sensing, Delft University of Technology
Stevinweg 1, 2628 CN Delft, The Netherlands

IGARSS 2021 - 2021 IEEE International Geoscience and Remote Sensing Symposium | 978-1-6654-0369-6/21/$31.00 ©2021 IEEE | DOI: 10.1109/IGARSS47720.2021.9554216

ABSTRACT

To retrieve the full displacement vector from InSAR, three line-of-sight (LoS) observations from different viewing geometries are required. However, often, at most two LoS observations are available. Within the literature, we encounter different approaches to address for this problem, unfortunately often with either mathematical or semantic flaws. Their impact reaches from quantitative errors in the reported studies, mismatches in comparative studies with other geodetic techniques, a lack of trust in the technology by end-users, to plain confusion. We propose both a uniform nomenclature and an alternative approach to the standard 3D decomposition problem using the concept of a strap-down reference system.

Index Terms— InSAR, surface displacements, line-of-sight, decomposition

1. INTRODUCTION

Satellite radar interferometry (InSAR) is a powerful technique for monitoring deformation phenomena. While deformation phenomena occur in a three-dimensional (3D) world, one of the limitations of the InSAR phase observations is that they are only sensitive to the projection of the 3D displacement vector onto the radar line-of-sight (LoS) direction [1]. The LoS projection d_{LoS} in a Cartesian east, north, up (ENU) coordinate system is given by

$$d_{\text{LoS}} = p_{\text{LoS}}\, d_{\text{ENU}} \tag{1}$$

where $p_{\text{LoS}} = [\sin\theta \sin\alpha_d, \sin\theta \cos\alpha_d, \cos\theta]$ is the projector onto the line of sight, and $d_{\text{ENU}} = [d_e, d_n, d_u]^T$ is the 3D displacement vector in east, north and up direction, respectively, θ is the incidence angle of the radar, and α_d is the azimuth of the zero-Doppler plane of the radar, at the position of the target.

Uniquely estimating the three displacement components would require at least three spatio-temporally coinciding independent (STCI) LoS observations, i.e., scatterers on an object that is not subject to internal deformations, observed at the same time. More importantly, the system of equations needs to have a full-rank coefficient matrix. Unfortunately, in most practical situations, at most two STCI LoS observations are available, resulting in an underdetermined system with an infinite amount of possible solutions.

Reviewing InSAR literature, we encounter different approaches to address the underdeterminancy, yet often with either mathematical or semantic flaws. Their impact reaches from quantitative errors in the reported studies, mismatches in comparative studies with other geodetic techniques, a lack of trust in the technology by end-users, to plain confusion. Here we classify the main categories of InSAR fallacies and analyze their impact.

Attribution errors: attributing the line-of-sight estimate completely to a vertical displacement, using a single viewing geometry. In such studies, no projection statements are given at al, and LoS observations are directly interpreted as vertical displacements ([2–7]). This is erroneous, and results in a severe underestimation (bias) of vertical displacements of up to 30%.

Projection errors: projecting the LoS displacement estimations onto the vertical, and subsequently presenting this as 'vertical displacements', or the equivalent situation in a particular horizontal direction. Occurs for a single viewing geometry. While *'projection onto the vertical'* would be a correct statement, *'vertical displacement'* is not, since the latter necessarily relies on the assumption that any non-vertical displacement component of the 3D vector is non-existent. While the term' projection onto the vertical' is in all cases correct, both geometrically as well as semantic, the term 'vertical displacement' can only be correctly interpreted if the assumption of a non-existent horizontal component is correct and explicitly mentioned. However, the assumption is often missing ([8–11]), and it is in many cases incorrect (e.g., for landslides and subsidence bowls). It leads to a biased estimation instead of a more noisy estimation, which often has a bigger impact and less chance of being detected ([12–18])

Decomposition errors: ignoring the null-space in the 3D solution space using only one or two viewing geometries, i.e., ascending and descending, and subsequently equating a 'non-measurable' displacement vector component to a 'non-existing' displacement vector component. In such cases, it is assumed that the *lack of sensitivity* in the north-south component for near-polar orbits is equivalent to the *absence* of a

north-south component by simply removing the component from the decomposition equation ([2, 19–27]). This assumption fails since the headings of the ascending and descending track are not completely symmetric and neglecting the north-south component results in biased estimates for the east-west and vertical component. Therefore, these approaches are very dependent on the actual magnitude of the north-south displacements.

Flawed assumptions. The problem of estimating 3D displacement vectors observed by only one or two viewing geometries can only be solved by adding additional information (conditions) in the form of assumptions. These need to be explicitly stated, both in the documentation and in the final products. Yet, in many cases, these assumptions are either *lacking, misstated, incorrect, or implausible.* The consequence of flawed assumptions typically results in biased results rather than noisy results.

2. METHODOLOGY

2.1. LoS-Vector decomposition using a local strap-down coordinate system

For most deformation phenomena we propose to work with a local, strap-down, right-handed Cartesian coordinate system which is fixed to the deformation phenomenon with transversal, longitudinal, and normal (TLN) components. A displacement in those three directions is projected to the LoS with Eq. (1) and [28]

$$d_{\text{ENU}} = R_1 R_2 R_3 d_{\text{TLN}}, \tag{2}$$

where d_{TLN} is the vector containing the displacement component in the strap-down system $d_{\text{TLN}} = [d_T, d_L, d_N]^T$, and R_1, R_2 and R_3 are rotation matrices which are expressed as

$$R_1 = \begin{bmatrix} \cos\beta & \sin\beta & 0 \\ -\sin\beta & \cos\beta & 0 \\ 0 & 0 & 1 \end{bmatrix}, \quad R_2 = \begin{bmatrix} 1 & 0 & 0 \\ 0 & \cos\gamma_l & -\sin\gamma_l \\ 0 & \sin\gamma_l & \cos\gamma_l \end{bmatrix},$$
$$R_3 = \begin{bmatrix} \cos\gamma_t & 0 & \sin\gamma_t \\ 0 & 1 & 0 \\ -\sin\gamma_t & 0 & \cos\gamma_t \end{bmatrix}, \tag{3}$$

where $\beta \in (0°, 360°]$ is the azimuth of the longitudinal direction relative to the north, $\gamma_l \in (-90°, +90°]$ is the slope in the longitudinal direction, and $\gamma_t \in (0°, +90°]$ is the slope in the transversal direction. The longitudinal direction is defined tangential to the local iso-elevation or iso-deformation lines, such that the positive transversal direction is always directed down-slope. The normal direction completes the right-handed system. The angles γ_t and γ_l represent the angles between the normal axis and the local zenith.

While Eq. (2) does not solve the problem of underdeterminancy, for many practical cases, e.g., line infrastructure, landslides, or subsidence bowls, analysis of the main driving forces supports the assumption that significant displacements in the longitudinal direction are unlikely. Under this assumption, (1) can be solved with two STCI LoS observations from sufficiently different viewing geometries.

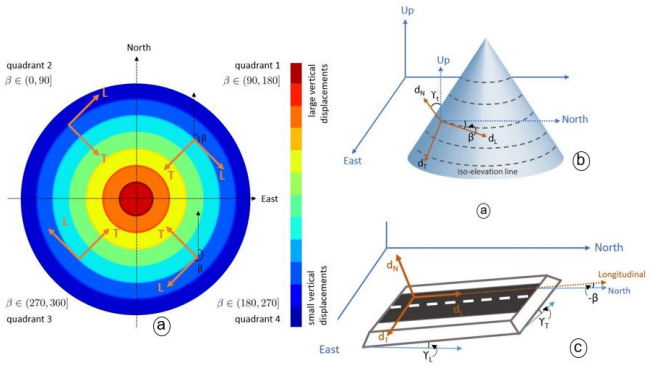

Fig. 1. The orientation of the local TLN strap-down coordinate system for different deformation phenomena. (a) subsidence bowl, (b) landslide and (c) line-infrastructure.

2.1.1. *Gravity-induced downslope deformation*

Landslides, moving glaciers, or slope instability are examples of phenomena where the main deformation occurs along the slope, with gravity as the main driving force. When the longitudinal axes is parallel to the iso-elevation lines of the slope of the occurring landslide, we can assume that displacements in the longitudinal direction are zero, i.e., all displacements occur in the vertical plane spanned by the d_T and d_U vectors, see Fig. 1b. The angle of the slope is γ_t, and $\gamma_L = 0°$ by definition. The slope aspect determines in further detail what the possible values are for the angles β and γ_t.

2.1.2. *Subsidence and uplift*

Subsidence bowls and uplift domes are caused by a change in volume underneath the Earth's surface. They exhibit vertical and horizontal displacement components. The horizontal component is orthogonal to the iso-deformation lines: centripetal for subsidence [29], and centrifugal for uplift. Thus, the longitudinal direction is oriented parallel to the iso-deformation lines, and the transversal direction is downslope (centripetal) for subsidence, see Fig. 1A. Due to the gravitational force, it is safe to assume that no displacements in the longitudinal direction may occur.

2.1.3. *Line-infrastructure*

Line infrastructure is characterized by an extended spatial dimension in one direction (the longitudinal direction), where the spatial extent in the other two directions is limited as for roads, railways, dikes, and pipelines. The slope of the asset is given by γ_l, and γ_t represents the cant of the asset or the

slope in the transversal direction, which is usually small. It is possible to assume that no significant deformations occur in the longitudinal direction [28]. For cases where γ_t equals zero, there is a directional ambiguity for β, and the smallest azimuth angle should be chosen, i.e., $\beta \in (-90°, 90°]$.

2.2. Mathematical and stochastic model

Under the assumption of zero longitudinal displacements, any displacement vector can be unambiguously represented in a 2D (d_T, d_N) system, as long as the orientation of the TLN frame is well chosen. However, the orientation of the frame needs to be estimated and any misalignment results in biased estimates for d_T and d_N. Therefore, the uncertainty of the frame alignment $(\sigma_\beta, \sigma_{\gamma_t}, \sigma_{\gamma_l})$ should be taken into account by adding pseudo observations $\underline{\beta}$, $\underline{\gamma_t}$ and $\underline{\gamma_l}$ for the orientation angles to the mathematical and functional model resulting in

$$\underbrace{\begin{bmatrix} \underline{d}^{(1)}_{\text{LoS}} \\ \vdots \\ \underline{d}^{(m)}_{\text{LoS}} \\ \underline{\beta} \\ \underline{\gamma_t} \\ \underline{\gamma_l} \end{bmatrix}}_{y} \} = \underbrace{\begin{bmatrix} a_1(x) \\ \vdots \\ a_m(x) \\ a_{m+1}(x) \\ a_{m+2}(x) \\ a_{m+3}(x) \end{bmatrix}}_{A(x)} = \underbrace{\begin{bmatrix} p_{1T}d_T + p_{1N}d_N \\ \vdots \\ p_{mT}d_T + p_{mN}d_N \\ \beta \\ \gamma_t \\ \gamma_l \end{bmatrix}}_{A(x)} \tag{4}$$

$$D\{ \underbrace{\begin{bmatrix} \underline{d}^{(1)}_{\text{LoS}} \\ \vdots \\ \underline{d}^{(m)}_{\text{LoS}} \\ \underline{\beta} \\ \underline{\gamma_t} \\ \underline{\gamma_l} \end{bmatrix}}_{y} \} = \underbrace{\begin{bmatrix} \sigma^2_{\text{LoS},1} & 0 & 0 & 0 & 0 & 0 \\ 0 & \ddots & 0 & 0 & 0 & 0 \\ 0 & 0 & \sigma^2_{\text{LoS},m} & 0 & 0 & 0 \\ 0 & 0 & 0 & \sigma^2_{\beta} & 0 & 0 \\ 0 & 0 & 0 & 0 & \sigma^2_{\gamma_t} & 0 \\ 0 & 0 & 0 & 0 & 0 & \sigma^2_{\gamma_l} \end{bmatrix}}_{Q_{yy}}, \tag{5}$$

where $E\{.\}$ expresses the expectation of the model, which can be solved with two STCI LoS observations, i.e., $\underline{d}^{(1)}_{\text{LoS}}$ and $\underline{d}^{(2)}_{\text{LoS}}$ and pseudo observations for the orientation angles. The unknowns of the model are $d_T, d_N, \beta, \gamma_t$ and γ_l. The first row in the A matrix is $[p_{1T}d_T + p_{1N}d_N]$ which corresponds to $p_{\text{LoS},1}R_1R_2R_3[d_T, d_L, d_N]^T$, with the component related to the longitudinal direction d_L removed. The projector differs per STCI LoS observation due to different incidence angles and the azimuth of the zero-Doppler plane at the target. The last three rows of $A(x)$ correspond to the pseudo observations for the orientation angles. $D\{.\}$ is the dispersion of the model, where $\sigma^2_{\text{LoS},1}$ and $\sigma^2_{\text{LoS},2}$ are the variances for the LoS observations. The mathematical model represented by Eqs. (4) and (5) is of full rank resulting in one unique solution. Since the model is non-linear, the solution can be found by using a Gauss-Newton iteration process.

3. RESULTS

We applied the strap-down approach at a case study in Norg (north of the Netherlands), where magnesium is extracted, resulting in a subsidence bowl. The area is monitored with Sentinel-1 data from ascending and descending acquisitions, where the mean incidence angles are $36.3°$ and $44.2°$, and the mean azimuths of the zero-Doppler planes are $261°$ and $98°$, respectively.

For different locations at the subsidence bowl, the orientation of the TLN frame is different. Therefore, we divided the full subsidence bowl into different regions of uniform motion (RUM's), see Fig. 2, and we assumed that all scatterers within one RUM behave according to the same deformation phenomenon. For every RUM, we estimated β and we set $\sigma_\beta = 5°$. We estimated $\gamma_t = 0°$ and $\gamma_l = 0°$ due to the absence of significant topography, and we set $\sigma_{\gamma_t} = 2°$ and $\sigma_{\gamma_l} = 2°$. Then, we computed the mean LoS displacement rates for both ascending and descending acquisitions ($v^{(1)}_{\text{LoS}}$ $v^{(2)}_{\text{LoS}}$), which serve as the observations together with estimates for the orientation of the frame in Eq. (4). Finally, we estimated the displacement velocities in both the transversal and normal direction, v_T and v_N, for every RUM with Eqs. (4) and (5), see Fig. 2. We also estimated the precision for the unknown velocities, visualized by ellipses around the transversal velocities and error bars for the normal velocities. The minor axes represent the uncertainty due to the uncertainty in the alignment of the frame. Further, it can be seen that the uncertainty for both the transversal velocity and the normal velocity differs per RUM, which is a result of the near-polar orbits of satellites. For such orbits, it is difficult to solve for the component in the north-south direction.

4. CONCLUSIONS

We found that working with an ENU reference system for the decomposition results in an underdetermined system. In the literature, we found different approaches to address this underdeterminancy, where it often lacks insight into the consequences of particular choices in terms of accuracy and precision. Also, in most of the approaches, biases on the components of the estimated deformation result from implicit assumptions that are not fulfilled. We propose a new systematic approach that gives more physically relevant estimates, and we were able to include the uncertainty of the TLN frame. The better we know the orientation angles, the better the precision for the unknown displacement parameters. The precision further depends on the orientation of the strap-down system. Using the strap-down approach results in more reliable estimates for the displacement components.

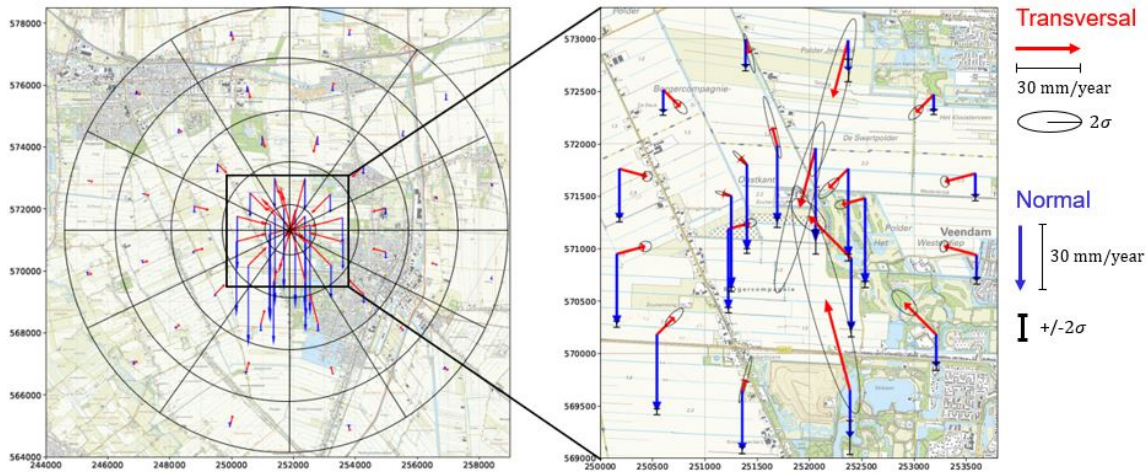

Fig. 2. Results when using the strap-down approach at a subsidence bowl which is the result of magnesium extraction at Norg. The red arrow's represent the estimated displacement velocities in the transversal direction, where their uncertainty is visualized by an ellipse. The blue arrows are the displacement velocities in the normal direction, which have an error bar.

References

[1] R. F. Hanssen, *Radar Interferometry: Data Interpretation and Error Analysis*. Dordrecht: Kluwer Academic Publishers, 2001.

[2] P. Teatini, L. Tosi, T. Strozzi, L. Carbognin, U. Wegmüller, and F. Rizzetto, "Mapping regional land displacements in the venice coastland by an integrated monitoring system," *Remote Sensing of Environment*, vol. 98, no. 4, pp. 403–413, 2005.

[3] S. Stramondo, F. Bozzano, F. Marra, U. Wegmuller, F. Cinti, M. Moro, and M. Saroli, "Subsidence induced by urbanisation in the city of rome detected by advanced insar technique and geotechnical investigations," *Remote Sensing of Environment*, vol. 112, no. 6, pp. 3160–3172, 2008.

[4] L. Solari, A. Ciampalini, F. Raspini, S. Bianchini, and S. Moretti, "Psinsar analysis in the pisa urban area (italy): a case study of subsidence related to stratigraphical factors and urbanization," *Remote Sensing*, vol. 8, no. 2, p. 120, 2016.

[5] M. Zheng, K. Deng, H. Fan, and S. Du, "Monitoring and analysis of surface deformation in mining area based on insar and grace," *Remote Sensing*, vol. 10, no. 9, p. 1392, 2018.

[6] L. Zhou, J. Guo, J. Hu, J. Li, Y. Xu, Y. Pan, and M. Shi, "Wuhan surface subsidence analysis in 2015–2016 based on sentinel-1a data by sbas-insar," *Remote Sensing*, vol. 9, no. 10, p. 982, 2017.

[7] M. Gao, H. Gong, B. Chen, X. Li, C. Zhou, M. Shi, Y. Si, Z. Chen, and G. Duan, "Regional land subsidence analysis in eastern beijing plain by insar time series and wavelet transforms," *Remote Sensing*, vol. 10, no. 3, p. 365, 2018.

[8] N. Short, A.-M. LeBlanc, W. Sladen, G. Oldenborger, V. Mathon-Dufour, and B. Brisco, "Radarsat-2 d-insar for ground displacement in permafrost terrain, validation from iqaluit airport, baffin island, canada," *Remote Sensing of Environment*, vol. 141, pp. 40–51, 2014.

[9] D. Raucoules, C. Maisons, C. Carnec, S. Le Mouelic, C. King, and S. Hosford, "Monitoring of slow ground deformation by ers radar interferometry on the vauvert salt mine (france): Comparison with ground-based measurement," *Remote sensing of environment*, vol. 88, no. 4, pp. 468–478, 2003.

[10] H. Sun, Q. Zhang, C. Zhao, C. Yang, Q. Sun, and W. Chen, "Monitoring land subsidence in the southern part of the lower liaohe plain, china with a multi-track ps-insar technique," *Remote sensing of environment*, vol. 188, pp. 73–84, 2017.

[11] S. Alatza, I. Papoutsis, D. Paradissis, C. Kontoes, and G. A. Papadopoulos, "Multitemporal insar analysis for monitoring ground deformation in amorgos island, greece," *Sensors*, vol. 20, no. 2, p. 338, 2020.

[12] W.-C. Hung, C. Hwang, Y.-A. Chen, L. Zhang, K.-H. Chen, S.-H. Wei, D.-R. Huang, and S.-H. Lin, "Land subsidence in chiayi, taiwan, from compaction well, leveling and alos/palsar: Aquaculture-induced relative sea level rise," *Remote Sensing*, vol. 10, no. 1, p. 40, 2018.

[13] A. H.-M. Ng, H. Wang, Y. Dai, C. Pagli, W. Chen, L. Ge, Z. Du, and K. Zhang, "Insar reveals land deformation at guangzhou and foshan, china between 2011 and 2017 with cosmo-skymed data," *Remote Sensing*, vol. 10, no. 6, p. 813, 2018.

[14] M. Haghshenas Haghighi and M. Motagh, "Sentinel-1 insar over germany: Large-scale interferometry, atmospheric effects, and ground deformation mapping," *ZfV: Zeitschrift für Geodäsie, Geoinformation und Landmanagement*, vol. 2017, no. 4, pp. 245–256, 2017.

[15] R. Bonì, F. Cigna, S. Bricker, C. Meisina, and H. McCormack, "Characterisation of hydraulic head changes and aquifer properties in the london basin using persistent scatterer interferometry ground motion data," *Journal of Hydrology*, vol. 540, pp. 835–849, 2016.

[16] W. Tang, P. Yuan, M. Liao, and T. Balz, "Investigation of ground deformation in taiyuan basin, china from 2003 to 2010, with atmosphere-corrected time series insar," *Remote Sensing*, vol. 10, no. 9, p. 1499, 2018.

[17] P. Milillo, G. Giardina, M. J. DeJong, D. Perissin, and G. Milillo, "Multi-temporal insar structural damage assessment: The london crossrail case study," *Remote Sensing*, vol. 10, no. 2, p. 287, 2018.

[18] R. N. Nof, G. Baer, A. Ziv, E. Raz, S. Atzori, and S. Salvi, "Sinkhole precursors along the dead sea, israel, revealed by sar interferometry," *Geology*, vol. 41, no. 9, pp. 1019–1022, 2013.

[19] B. V. Yazici and E. Tunc Gormus, "Investigating persistent scatterer insar (psinsar) technique efficiency for landslides mapping: a case study in artvin dam area, in turkey," *Geocarto International*, pp. 1–19, 2020.

[20] H. Klemm, I. Quseimi, F. Novali, A. Ferretti, and A. Tamburini, "Monitoring horizontal and vertical surface deformation over a hydrocarbon reservoir by psinsar," *First break*, vol. 28, no. 5, 2010.

[21] A. Rucci, D. Vasco, and F. Novali, "Monitoring the geologic storage of carbon dioxide using multicomponent sar interferometry," *Geophysical Journal International*, vol. 193, no. 1, pp. 197–208, 2013.

[22] C. Janna, N. Castelletto, M. Ferronato, G. Gambolati, and P. Teatini, "A geomechanical transversely isotropic model of the po river basin using psinsar derived horizontal displacement," *International Journal of Rock Mechanics and Mining Sciences*, vol. 51, pp. 105–118, 2012.

[23] S. Yun, P. Segall, and H. Zebker, "Constraints on magma chamber geometry at sierra negra volcano, galápagos islands, based on insar observations," *Journal of Volcanology and geothermal research*, vol. 150, no. 1-3, pp. 232–243, 2006.

[24] K. Pawluszek-Filipiak and A. Borkowski, "Integration of dinsar and sbas techniques to determine mining-related deformations using sentinel-1 data: The case study of rydułtowy mine in poland," *Remote Sensing*, vol. 12, no. 2, p. 242, 2020.

[25] A. Tamburini, M. Bianchi, C. Giannico, and F. Novali, "Retrieving surface deformation by psinsar™ technology: A powerful tool in reservoir monitoring," *International Journal of Greenhouse Gas Control*, vol. 4, no. 6, pp. 928–937, 2010.

[26] D. H. T. Minh, N. Yen-Nhi, T. T. Lê, T. C. Le, H. S. Bui, Q. V. Vuong, and T. Le Toan, "Quantifying horizontal and vertical movements in ho chi minh city by sentinel-1 radar interferometry," 2020.

[27] S. Alatza, I. Papoutsis, D. Paradissis, C. Kontoes, G. A. Papadopoulos, and C. Raptakis, "Insar time-series analysis for monitoring ground displacement trends in the western hellenic arc: The kythira island, greece," *Geosciences*, vol. 10, no. 8, p. 293, 2020.

[28] L. Chang, R. P. Dollevoet, and R. F. Hanssen, "Monitoring line-infrastructure with multisensor sar interferometry: products and performance assessment metrics," *IEEE journal of selected topics in applied earth observations and remote sensing*, vol. 11, no. 5, pp. 1593–1605, 2018.

[29] D. Müller and A. Preusse, "Use of the area of main influence to fix a relevant boundary for mining damages in germany," *International Journal of Mining Science and Technology*, vol. 28, no. 1, pp. 79–83, 2018.